$Al_2Mo_3O_{12}$/polyethylene composites with reduced coefficient of thermal expansion

Alexandre Roberto Soares,[†] *Patricia I. Pontón,*[Ψ] *Lidija Mancic,* [§] *José R. M. d'Almeida,*[Ψ] *Carl P. Romao,*[Л, ‡] *Mary Anne White,*[Л, ‡,ξ] *Bojan A. Marinkovic*[†, Ψ *]

[†]Centro Universitário de Volta Redonda – UNIFOA, Av. Paulo Erlei Alves Abrantes 1325, Volta Redonda – RJ, Brasil

[Ψ]Departamento de Engenharia de Materiais, Pontifícia Universidade Católica de Rio de Janeiro – PUC-Rio, Rua Marquês de São Vicente 225, Gávea, Rio de Janeiro, RJ, Brasil

[§]Institute of Technical Sciences of SASA, Knez Mihailova 35/IV, Belgrade, Serbia

[Л]Department of Chemistry, Dalhousie University, Halifax, Nova Scotia, B3H 4R2, Canada

[‡]Institute for Research in Materials, Dalhousie University, Halifax, Nova Scotia, B3H 4R2, Canada

[ξ]Department of Physics and Atmospheric Sciences, Dalhousie University, Halifax, Nova Scotia, B3H 4R2, Canada

e-mail addresses:

alexandresoares@inb.gov.br

patriciapontonb@aluno.puc-rio.br

lidija.mancic@itn.sanu.ac.rs

dalmeida@puc-rio.br

cpr@dal.ca

mary.anne.white@dal.ca

bojan@puc-rio.br*

Corresponding author. Tel: +55-21-35271954; fax: +55-21-35271236
E-mail address: bojan@puc-rio.br (B.A. Marinkovic)

Abstract

Recently, polymer composites reinforced with lowfractions of thermomiotic nanoceramics have triggered a lot of research. The efforts have been focused on achieving considerable reduction of the coefficient of thermal expansion (CTE) of polymeric materials without deterioration of other physical properties. In this context, polyethylene (PE) composites reinforced with different loads of $Al_2Mo_3O_{12}$ nanofillers (0.5 to 4 mass %) were fabricated by micro-compounding. To enhance the interfacialinteraction between the two components chemical functionalization of $Al_2Mo_3O_{12}$ was performed with vinyltrimethoxysilane (VTMS) prior to micro-compounding. Infrared spectroscopy and thermogravimetry demonstrated the successful grafting of VTMS on the $Al_2Mo_3O_{12}$ surface. The composites showed strongly decreased CTEs, up to 46 % reduction for loadings of 4 mass % compared with neat PE, suggestingintimate filler-matrix interactions. The variation of CTEs of the composites in terms ofthe fillerfraction was successfully described by Turner's model allowingcalculation ofthe bulk modulus of monoclinic $Al_2Mo_3O_{12}$ (13.6± 2.6 GPa),in agreement with the value obtained by an ultrasonic method. The thermal stability of thecomposites was improved, although the addition of functionalized fillers decreased the degree of crystallinity of the PE to a small extent. The Young's modulus and yield strength of the compositesincreased from6.6 to 19.1 % and 4.0 to 6.0 %, respectively, supporting the existence of strong filler-matrix interactions, contributing to an efficient load transfer. Finite element analysis of thermal stresses indicated absence of plastic deformation of the matrix or fracture of thenanofillers, for a 100 K temperature drop.

Keywords: negative thermal expansion,ceramics, bulk modulus, thermoplastics, chemical functionalization, nanomaterials.

1. Introduction

Negative thermal expansion (NTE) ceramics, also known as thermomiotics[1], began to attract significant attention in the 1990s due to newly discovered phases exhibiting this uncommon thermal expansion feature [2-4]. Since then, considerable research has been carried out to advance understanding of the physics underlying this phenomenon [5-8], while parallel efforts have been made to transform this new class of compounds into useful materials. There are two general tentative approaches to engineer new materials based on thermomiotics. One route corresponds to the development of bulk monolithic ceramics with well-defined CTEs, generally free of undesired microstructural defects (microcracks) and frequently aiming at near zero values [9]. However, in some cases, such as Al_2TiO_5, microstructural design and microcrack formationcan be used to advantage to produce low thermal expansion materials with high thermal shock resistance [10]. On the other hand, the second approach makes use of the addition of thermomiotics, as the dispersed phase, in composites [11-29]. The most common role of thermomiotics in composites is to control the CTE of the matrix phase, which could be a metal, ceramic or polymer.

Thermoplastic polymers generally present very poor dimensional stability on temperature variation. Therefore, the addition of inorganic fillers with low positive, near zero or negative CTEs can mitigate high CTEs in polymers, while direct or silane crosslinking strategies are also employed in order to improve their physical properties. An example of the importance of controlling thermal expansionin polymers is observed in the field of electronic packaging polymers, such as polystyrene [30]and thermoset epoxy resins [31], applied over integrated circuit chips to protect them from environmental factors. These polymers are usually filled with a ceramic showing low CTE and moderate thermal conductivity for the sake of reduction of thermal mismatch between the packaging polymer and the substrate, while also increasing the thermal conductance of the package layer. Polyethylene (PE) is one of the most used thermoplastics. Geomembranes and pipes for water or natural gas transmission/distribution are some examples of PE applications where the huge CTE (~ 10^{-4} K^{-1}) or migration of volatile organic components (VOCs) can induce material damage orlead to poor performance [32, 33]. The list of dispersed phases studied for the purpose of reduction of CTE of PE is extensive and includes clays, $CaCO_3$, Si, fly ash, CeO_2, $Sr_2Al_2SiO_7$, just to mention a few [34-39], but, so far, has not included thermomiotics or low CTE materials.

Regarding thermomiotic fillers, there are only a few reports in the literature of attempts to control the CTE of polymers, mostly thermosetting matrices. Thesetentativeattemptsgenerally focus on ZrW_2O_8, both as micronic and nanometric powders [11, 15-17, 23-25]. This is understandable considering the isotropic physical properties of $ZrW_2O_8$and its strong negative CTE (~ - 9 x 10^{-6} K^{-1}) over a wide temperature range (0-1050K), which includes theoperational temperature range for polymer components. This NTE material has been used for the reduction of CTE of polyimide, polyester and epoxy resin [11,15-17,23,24], while, as far as the authors are aware, there are no reports on its use in a PE matrix. On the other hand, the thermomiotics and low CTE compounds from the $A_2M_3O_{12}$ family are rarely cited in the literature as the dispersed phases for controlling CTE in composites [14, 18, 19, 22, 40].An advantage of the compounds from this family is their wide chemical flexibility, resulting in a variety of orthorhombic phases with CTEs ranging between – 11 x 10^{-6} and 2 x 10^{-6} K^{-1} [8, 41, 42]. Even in the monoclinic phase, the magnitude of the CTE of $A_2M_3O_{12}$ compounds is low [9]. It is also significant that some of the $A_2M_3O_{12}$ compounds are routinely synthesized from inexpensive reagents,which is not the case for ZrW_2O_8 and related compounds. There are currently just a few reports of the application of $A_2M_3O_{12}$ compounds as fillers in ceramic-ceramic (MoO_3, ZrO_2, $ZrSiO_4$ and ZrW_2O_8 featuring as matrices) [14, 19, 22, 40]and ceramic-metal (Mg and Cu matrices) [18, 40]composites. However, there are no reports on the use of $A_2M_3O_{12}$ in polymer matrices. The $A_2M_3O_{12}$ compounds already tested in composites as dispersed phases are $Y_2W_3O_{12}$, $Sc_2W_3O_{12}$, $Fe_xSc_{1-x}W_3O_{12}$ and $ZrWP_2O_{12}$, while the application of $Al_2Mo_3O_{12}$ was only reported in the monolithic form [9].

The principal purpose of this study was to examine the viability and potential employment of a nanometric-sized $A_2M_3O_{12}$ as a filler for thermoplastic matrices, added in low amounts (≤ 4 mass %), to reduce the CTE of thermoplastic polymers without provoking adverse effects on their mechanical properties and thermal stability. Because of its technological appeal, PE has been chosen as the matrix, while $Al_2Mo_3O_{12}$, a reasonably well studied material[9, 43, 44], has been elected as the nanofiller, although in the temperature range below 473 K it adopts the monoclinic form with a low positive CTE [9]. To enhance the interface interaction between the inorganic hydrophilic filler and the hydrophobic polyolefin matrix, chemical functionalization of $Al_2Mo_3O_{12}$ nanoparticles was carried out with the aid of a bi-functional coupling agent, vinyltrimethoxysilane (VTMS). One functional group of VTMS is hydrolysable

trimethoxysilane (–($Si(OCH_3)_3$)), which is capable of establishing primary bonds with the surface of the inorganic filler, while the other functional group is a hydrophobic vinyl group (CH_2=CH-), capable of interacting physically (inter-molecular entanglement) or chemically, through primary bonds created in the presence of peroxide initiators, with PE chains. The composites were processedby micro-compounding,includingextrusion and injection molding.

2. Materials and methods

2.1 Materials

Starting reagents for synthesis of $Al_2Mo_3O_{12}$ nanopowder and its functionalization include $Al(NO_3)_3 \cdot 9H_2O$ (Isofar, 99 %), $(NH_4)_6Mo_7O_{24} \cdot 4H_2O$ (Isofar, 99 %), NaOH (Vetec, 99 %), vinyltrimethoxysilane $C_5H_{12}O_3Si$ (Evonik, 98%), acetic acid (Vetec) and anhydrous ethanol (Sigma Aldrich). All reagents were used asreceived. Granulated medium density PE (MR-435, Braskem) with a density of 0.934 gcm^{-3} and melt flow index (MFI) of 4.0 g/10 min served as the matrix.

The synthesis and characterization of $Al_2Mo_3O_{12}$ nanopowder through a co-precipitation route is described in detail elsewhere[9].

Bulk $Al_2Mo_3O_{12}$ pellets were prepared in order to measure their mechanical properties using ultrasonic transduction. Thesynthesis was performed using a solid-state reaction method, using Al_2O_3 (Sigma-Aldrich, 99.7 %) and MoO_3 (Sigma-Aldrich, 99.5 %) as precursors. The precursor powders were mixed and mechanically activated in a high-energy ball mill for 12 hours, followed by consolidation in a cylindrical die press (15 mm diameter) under approximately 55 MPa of pressure and subsequent reactive sintering for 24 h at 1050 K in air. The three resulting pellets had an average height of 4.78 mm and a density fraction 73 % of theoretical.

2.2 Functionalization of $Al_2Mo_3O_{12}$ nanoparticles with VTMS

The functionalization of $Al_2Mo_3O_{12}$ was carried out using 51 mL of ethanol/water 95:5 % v/v as the reaction medium[45]. A mass of 1g of $Al_2Mo_3O_{12}$, obtained though the co-precipitation route and ground into a fine powder, was added to aqueous ethanol and stirred for 10 min, while the pH was adjusted with acetic acid to 4.5-5.5. The suspension was placed in an ultrasonic bath for 1 h and the pH was adjusted again to 4.5-5.5. VTMS was added dropwise until a mass ratio of 1:2 (VTMS: $Al_2Mo_3O_{12}$) was reached. This suspension was mechanically stirred at a frequency of 5000 min^{-1} (Ultra Turrax Ika T25 disperser) for 2 h, then ultrasonicated for a further 1 h. The as-grafted $Al_2Mo_3O_{12}$ nanoparticles were washed three times with aqueous ethanol

to remove the excess VTMS, and then filtered and dried at 383 K for 2 h in an air-circulating oven. Here the silanized $Al_2Mo_3O_{12}$ nanoparticles are referred to as "VTMS-g-$Al_2Mo_3O_{12}$", where "g" denotes that VTMS was grafted onto the nanoparticle surfaces.

2.3 Preparation of VTMS-g-$Al_2Mo_3O_{12}$/PE composites

VTMS-g-$Al_2Mo_3O_{12}$/PE composites were prepared in a twin-screw micro-extruder (DSM Xplore 5cc Microcompounder). The screw speed was 100 rpm, the barrel temperature profile 443, 448 and 453 K (from the top to the bottom) and the mixing time was approximately 5 min. The extrudate was fed to a micro-injection molding machine (DSM Xplore 5.5 cc) to obtain ASTM D638-10 tensile specimens. The injection pressure was set to 7 bar. The melt and mold temperatures were kept at 448 K and 353 K, respectively. To investigate the effect of different loads of VTMS-g-$Al_2Mo_3O_{12}$ on CTE, thermal stability and mechanical properties of PE,composites containing nominally0.5, 1.0, 2.0, 3.0 and 4.0 mass % of VTMS-g-$Al_2Mo_3O_{12}$ were prepared and compared with neat PE specimens.

2.4 Characterization

2.4.1 $Al_2Mo_3O_{12}$ powder

The $Al_2Mo_3O_{12}$ powder obtained through co-precipitation was characterized by X-ray powder diffraction (XRPD) on a Siemens D5000 using CuK_α radiation in steps of 0.02^o (8 s per step) from 10^o to 60^o (2 *theta*) to determine phase composition of the product and to evaluate the average crystallite size of $Al_2Mo_3O_{12}$. Powder Diffraction File 2 Release 2011(PDF-2) was used for crystal phase identification, while Topas 4.2 was used for LeBail analysis. The direct convolution approach, embedded in Topas 4.2, has been used in order to separate physical from instrumental contributions within the experimental pattern. The instrumental contribution has been described through the Fundamental Parameter Approach (FPA), while the physical (microstructural) contribution was modelled by two Voigt functions. The reported crystal size parameter is LVOL-IB obtained from the integral breadth of the Voigt function that describes crystallite size contribution to the physical broadening. This approach for determination of crystallite sizes is known as the Balzar method.

Transmission electron microscopy (TEM) was performed on a JEOL-2010 microscope operating at 200 kV using a Gatan CCD camera. TEM specimens were prepared by dispersing the powder samples in isopropyl alcohol via ultrasonic treatment and then dropped onto a porous carbon film supported by a copper grid. Powder

samples, following pretreatment at 393 K under vacuum (50 mTorr), were characterized by N_2 adsorption at 77 K on a Micromeritics TriStar 3000V6.03 instrument. Specific surface area was calculated using the Brunauer–Emmett–Teller (BET) equation in the P/P_o range of 0.06–0.21.

2.4.2 Bulk $Al_2Mo_3O_{12}$

The transverse and longitudinal velocities of sound in three $Al_2Mo_3O_{12}$ pellets were measured ultrasonically using a Panametrics 25D Ultrasonic Thickness Gauge with Panametrics shear-wave couplant and glycerol (longitudinal-wave couplant). The measured velocities of sound were corrected for porosity as follows [46]:

$$v = v_0(1 - p), \quad (1)$$

where v is the measured velocity, v_0 is the corrected, fully densified, velocity, and p is the pore fraction.

2.4.3 VTMS-g-$Al_2Mo_3O_{12}$

Fourier transform infrared spectroscopy (FTIR) was performed in the range 4000 to 500 cm^{-1}, using pellets with the addition of dried IR-grade KBr,in a Perkin-Elmer Spectrum 100 FT-IR spectrometer with a resolution of 0.5 cm^{-1}.

Thermogravimetric analyses (TGA) were carried out on a Perkin-Elmer Simultaneous Thermal Analyzer (STA-6000). About 5 mg of VTMS-g-$Al_2Mo_3O_{12}$ was added to an alumina pan (180 μL) and heated in N_2 gas flux (50 $mLmin^{-1}$) in the temperature range between 298 and 853 K, at a heating rate of 10 $Kmin^{-1}$. The thermogravimetric balance was previously calibrated in N_2 gas flux (50 mL min^{-1}) in the range between 298 K and 1173 K using a 15 mg of $CaC_2O_4 \cdot H_2O$ standard sample, supplied by Perkin-Elmer. The buoyancy effect, observed in TG curves (as a small mass gain, < 0.1 mass %, at temperatures lower than 330 K),was partially corrected by blank tests. Both analyses, FTIR and TGA, were also performed on $Al_2Mo_3O_{12}$ powder before grafting, for comparison.

2.4.4 VTMS-g-$Al_2Mo_3O_{12}$/PE composites

Dilatometric curves of neat PE and VTMS-g-$Al_2Mo_3O_{12}$/PE composites were determined in air atmosphere using a NETZSCH dilatometer DIL 402C in the temperature range from 298 to 373 K with a heating rate of 10 $Kmin^{-1}$. The specimens for dilatometry were prismatic rods (3.3 mm × 3.2 mm × 11 mm) manufactured from the injection molded specimens. Each material, neat PE and VTMS-g-$Al_2Mo_3O_{12}$/PE composites, was tested using threeseparate samples. The instrument was assessed for

accuracy using an α-alumina rod supplied by NETZSCH. The accuracy of $\Delta L/L_o$ (thermal strain; L_o is the original sample length) is ~ 1 % for the dilatometer used [47].

TGA and differential scanning calorimetry (DSC) analyses were carried out on the equipment described in section 2.4.3 using the same conditionsand corrections, but in the temperature range 298 to 923 K.Simultaneous Thermal Analyzer (STA-6000) was calibrated for temperature and enthalpy using ~ 5 mg of indium and silver standard samples, supplied by Perkin-Elmer. TG curves of neat PE and VTMS-g-$Al_2Mo_3O_{12}$/PE composites are reported in the Online Resource.

Tensile tests were carried out on ASTM D638-10 tensile specimens, at room temperature, on an EMIC Universal Testing Machine (model DL 1000) with the crosshead speed separation of 30 mm/min. Each material (neat PE and VTMS-g-$Al_2Mo_3O_{12}$/PE composites) was tested using sixseparate specimens.

2.4.5 Finite element analysis

Finite element analysis (FEA) was used to assess the thermal stress that could be expected in VTMS-g-$Al_2Mo_3O_{12}$/PE composites upon cooling. The COMSOL Multiphysics 4.4 software package was used to perform the analysis. The model geometry chosen was that of nine spherical filler particles of monoclinic $Al_2Mo_3O_{12}$ embedded at random positions in a cube of PE, where the volume fraction of filler was varied to match the experimental compositions.A mesh of tetrahedral elements was generated in COMSOL and the mesh size used was shown by a mesh convergence study to produce results convergent to within 1%.

The VTMS grafting was assumed, based on the experimental results described below, to produce perfect interfaces between matrix and filler.Both $Al_2Mo_3O_{12}$ and PE were treated as linear elastic materials. Assumption of perfect interfaces and linear elasticity leads to the calculated stress being a conservative estimate; the stress in the actual composite could be reduced by imperfect interfaces or ductility. Therefore, the results of the finite element analysis should be treated as qualitatively accurate.Due to the low volume fractions of filler used, the size, shape, and distribution of the particles did not substantially influence the results and these parameters were not varied as part of this study. The boundary conditions used were a temperature drop of 100 K on all sides of the material and roller boundaries on three perpendicular sides.

3. Results

3.1 $Al_2Mo_3O_{12}$ powder

The experimental XRPD pattern (Figure 1) confirmed that the co-precipitation route resulted in a single-phase powder, since all diffraction lines correspond to monoclinic $Al_2Mo_3O_{12}$ (PDF: 01-089-8579). However, the well-defined diffraction lines of monoclinic $Al_2Mo_3O_{12}$were overlaid on a broader diffraction pattern. A thorough examination of the powder by TEM revealed an intimate mixture of well-defined nanometric crystals (50 to 200 nm) with much smaller nanocrystallites(ca. 10 nm); see Figure 2. (A few other TEM images presented in Online Resource illustrate the presence of larger particles.)This observation was confirmed more quantitatively by applying LeBail analysis considering two $Al_2Mo_3O_{12}$ phases with the same monoclinic structure but different mean crystal sizes (Figure 1). Only this fitting approach resulted in good agreement with the experimental pattern, giving average crystal sizes of 70 nm for the well-defined $Al_2Mo_3O_{12}$ and 10 nm for the broader $Al_2Mo_3O_{12}$ diffraction pattern. BET analysis of N_2 adsorption indicated a specific surface area of 8.4 m^2g^{-1}.Considering a crystallographic density of 3.495 g cm^{-3} for monoclinic $Al_2Mo_3O_{12}$ [9], an average (spherical) particle size of ~ 100 nm was calculated from the observed specific surface area (8.4 m^2 g^{-1}), which is somewhat larger than the crystallite sizes obtained from XRPD data.

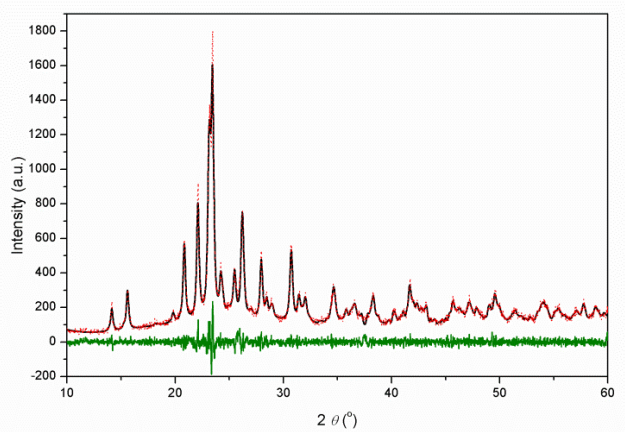

Fig.1 Experimental XRPD patternof monoclinic $Al_2Mo_3O_{12}$ (red dotted line), the pattern fit bythe Le Bail method (black line) and the difference plot (green line)

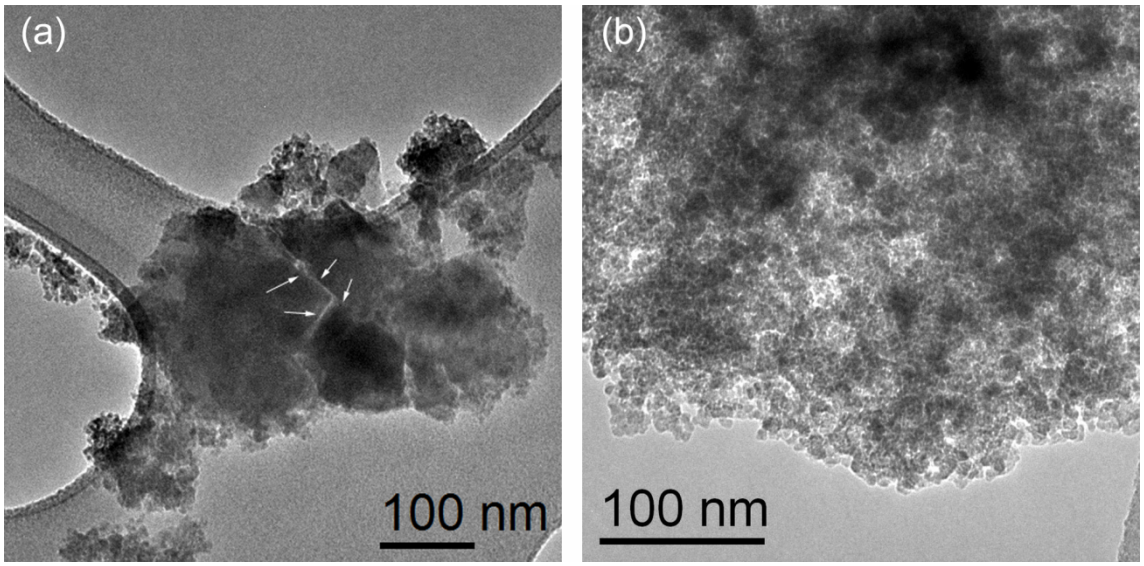

Fig.2 TEM images of $Al_2Mo_3O_{12}$ nanometric powdershowing a mixture of crystal sizes (a) from 50 to 200 nm(arrows indicate faces of larger particles)and (b) ~10 nm

3.2 Bulk $Al_2Mo_3O_{12}$

Following correction for porosity (Eq. 1), the longitudinal velocity of sound of monoclinic $Al_2Mo_3O_{12}$ was determined as 3.29 ± 0.16 m $ms^{-1}$and the transverse velocity of sound was determinedas 2.29 ± 0.22 m ms^{-1}. Using the reported theoretical density of monoclinic $Al_2Mo_3O_{12}$ of 3.495 g cm^{-3}[9], these values correspond to a bulk modulus of 13.5 ± 1.3 GPa and a shear modulus of 18.2 ± 0.7 GPa. Interestingly, this indicates that monoclinic $Al_2Mo_3O_{12}$ has a near-zero Poisson ratio, specifically 0.036 ± 0.088.

3.3 VTMS-g-$Al_2Mo_3O_{12}$

FTIR spectra of pristine $Al_2Mo_3O_{12}$ and VTMS-g-$Al_2Mo_3O_{12}$ are presented for comparison in Figure 3.

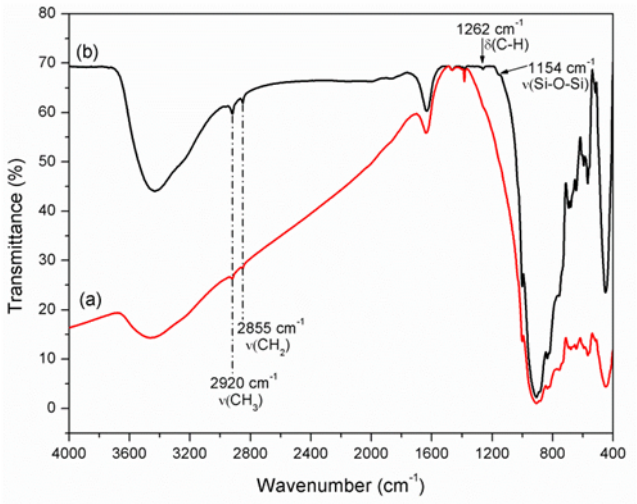

Fig.3 FTIR spectra of (a) pristine $Al_2Mo_3O_{12}$ and (b) VTMS-g-$Al_2Mo_3O_{12}$

The spectrum of VTMS-g-$Al_2Mo_3O_{12}$ shows four absorption bands at 2920, 2855, 1262 and 1154 cm^{-1} that suggest grafting of VTMS onto $Al_2Mo_3O_{12}$. The bands at 2920 and 2855 cm^{-1} are generally assigned to stretching vibration modes (ν) of CH_3 in (OC_2H_5) and CH_2 in ($CH{=}CH_2$) [48], respectively, while the band at 2920 cm^{-1} is also attributed to stretching vibration modes of CH_3 in (OCH_3) [49, 50]. However, these two bands at 2920 and 2855 $cm^{-1}$are also faintly observable in the spectrum of pristine $Al_2Mo_3O_{12}$ and are attributed to organic surface contamination [51]. The band at 1262 cm^{-1} appears only in the VTMS-g-$Al_2Mo_3O_{12}$ spectrum and is assigned to the in-plane CH bendingmode (δ) in ($CH{=}CH_2$) [48]. In addition, there is a band at 1154 cm^{-1} attributed to ν(Si-O-Si) [52], proving the occurrence of oligomerization between silanol reaction groups grafted on the $Al_2Mo_3O_{12}$ nanoparticles.

From the TGA results, a total mass loss of ~ 1.1 mass% of pristine $Al_2Mo_3O_{12}$ from room temperature up to 853 K (Figure 4) was observed and is attributed to physically adsorbed water (moisture) and primary bonded hydroxyl groups[53].

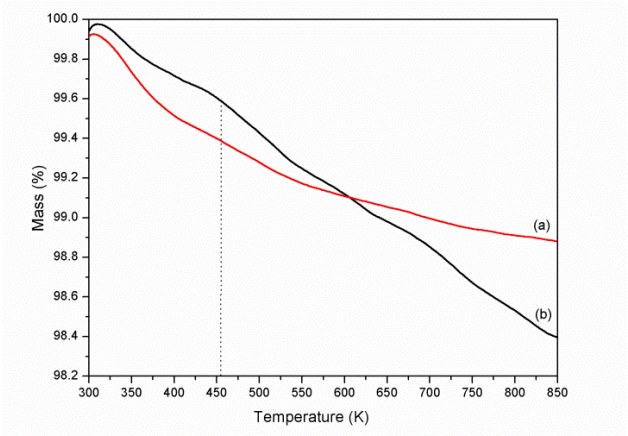

Fig.4 TG curves of (a) pristine $Al_2Mo_3O_{12}$ and (b) VTMS-g-$Al_2Mo_3O_{12}$

It is considered that desorption of moisture takes place up to ~ 453 K (Figure 4), while above this temperature the dehydration of primary bonded hydroxyl groups is the predominant mass loss process [53]. On the other hand, the total mass loss of VTMS-g-$Al_2Mo_3O_{12}$ is ~ 0.5 mass % more than for pristine $Al_2Mo_3O_{12}$ for the same temperature interval (298 K – 853 K), corroborating grafting of VTMS on $Al_2Mo_3O_{12}$. It is worth noting that up to 453 K (see Figure 4) the mass loss of VTMS-g-$Al_2Mo_3O_{12}$ is lower than for pristine $Al_2Mo_3O_{12}$, indicating that the moisture content in VTMS-g-$Al_2Mo_3O_{12}$ is lower due to its more hydrophobic nature.Furthermore, the mass loss between 453 K and 853 K (~ 1.2 mass %) is predominantly due to the release of the VTMS fragments, possibly vinyl groups, grafted on $Al_2Mo_3O_{12}$ nanoparticles [53]. This could be indirect evidence for primary bonding between Si from reactive silanol [53] and the surface of $Al_2Mo_3O_{12}$ through Si-O-Al and/or Si-O-Mo linkages. The successive processes of hydrolysis, oligomerization and grafting, through the condensation of VTMS onto the surface of $Al_2Mo_3O_{12}$ nanoparticles, are presented in Figure 5.

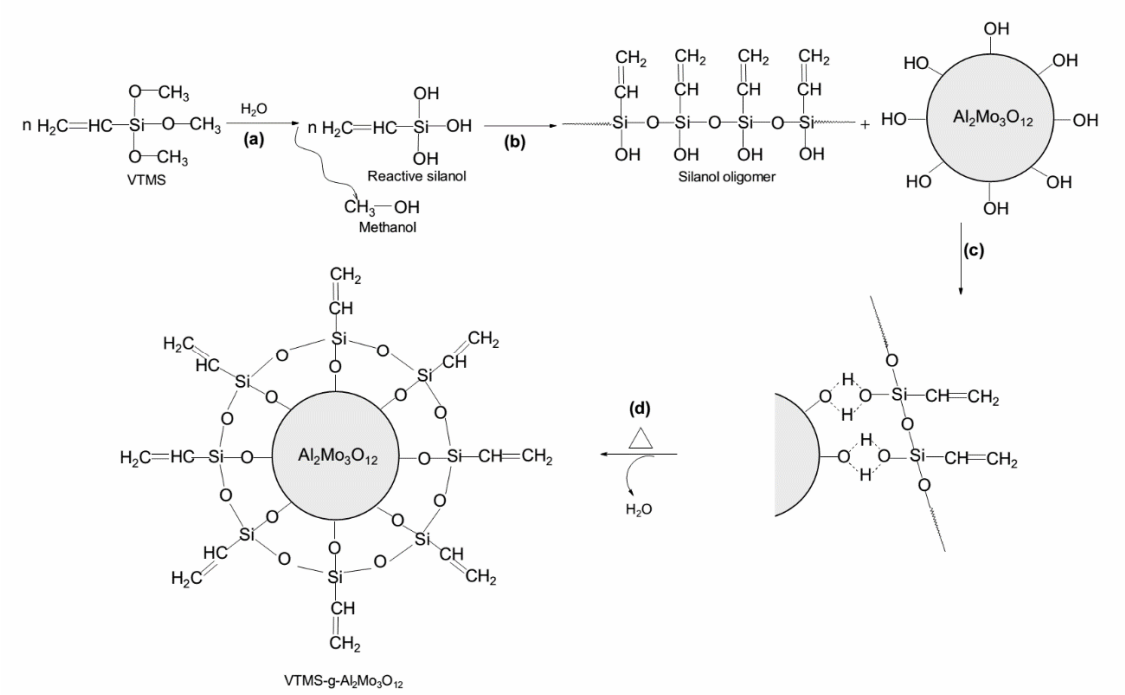

Fig.5 Scheme of (a) hydrolysis of VTMS; (b) oligomerization of reactive silanol molecules; (c) formation of hydrogen bonds between silanol oligomers and $Al_2Mo_3O_{12}$ nanoparticles and (d) grafting of VTMS on $Al_2Mo_3O_{12}$ surface through primary bonds

3.4 VTMS-g-$Al_2Mo_3O_{12}$/PE composites: Coefficient of thermal expansion, thermal stability and mechanical properties

CTEs of neat PE and VTMS-g-$Al_2Mo_3O_{12}$/PE composites were calculated from the slopes of the respective thermal strain curves in the temperature range between 303 K and 373 K (Table 1).

Table 1. Thermal properties and degree of crystallinity of VTMS-g-$Al_2Mo_3O_{12}$/PE composites with different filler contents. Nominal filler contents are presented; TGA shows inhomogeneity of the order of ±0.5 mass %, regarding to nominal contents, for the samples used in dilatometry. CTE values are standard deviations based on triplicate measurements.

Filler content(mass %)	CTE (x10^{-4} K^{-1})	Mass loss (%) up to 573 K	Mass loss (%) up to 673 K	T_{10}(K)	T_{50} (K)	T_m (K)	X_c (%)
0.0	2.290± 0.0005	0.90	1.95	722	749	414	76
0.5	1.98± 0.26	0.07	0.88	728	751	415	73
1.0	2.12± 0.31	0.13	1.02	726	750	414	70
2.0	1.80± 0.29	0.02	0.84	727	751	415	73
3.0	1.78± 0.04	0.0	0.91	721	749	412	74
4.0	1.23 ± 0.11	0.0	0.53	729	752	413	75

Large reductions of CTE, in comparison to neat PE, have been shown for almost all VTMS-g-$Al_2Mo_3O_{12}$/PE blends (0.5 - 4 mass %of filler), reaching a reduction of ~ 46% for a loading of 4 mass %. The observed dependence of the average experimental CTEs (Table 1) and volume fraction of VTMS-g-$Al_2Mo_3O_{12}$ filler (Figure 6) can be successfully described by Turner's model[15]:

$$\alpha_c = \frac{\alpha_m K_m (1-\emptyset) + \alpha_f K_f \emptyset}{K_m (1-\emptyset) + K_f \emptyset} \quad , \qquad (2)$$

where K_m and K_f are the bulk moduli of PE (matrix) and $Al_2Mo_3O_{12}$ (filler), $\emptyset$ is the volume fraction of filler, and α_c, $\alpha_m$and α_f are theCTEs of the composite, PE (matrix) and $Al_2Mo_3O_{12}$ (filler), respectively. Other models, such as the rule of mixtures, and those of Schapery, Vo or Kerner, have not been able to model the experimental dependence on average CTEs of the composites on volume fraction of filler.

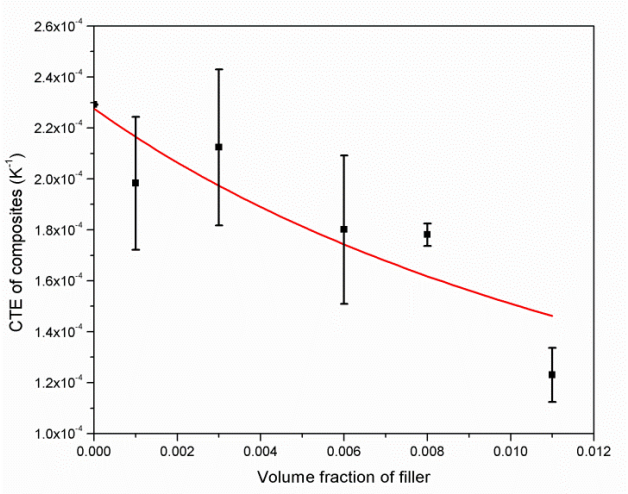

Fig.6 Average experimental CTEs of VTMS-g-$Al_2Mo_3O_{12}$/PE composites, with standard deviation bars, as a function ofnominal volume fraction of filler(black squares) fitted by Turner's model (red curve). Standard deviation bar for neat PE is smaller than the symbol.

The literature valueof $\alpha_f = 9.5 \times 10^{-6}$ $K^{-1}$was considered for monoclinic $Al_2Mo_3O_{12}$[9], while α_m (PE) was taken from Table 1 ($\alpha_m = 2.29 \times 10^{-4}$ K^{-1}). The bulk modulus of PE (K_m) was estimated as 0.278 GPafrom the mean value of Young's modulus (E_m = 0.278 GPa) measured for neat PE (Figure 7), assuming:

$$\mu_m \sim \frac{3}{8} E_m \quad , \qquad (3)$$

where μ_m is shear modulus of matrix, and

$$K_m = \frac{E_m \mu_m}{3(3\mu_m - E_m)}. \quad (4)$$

Considering these values it is possible, using the Turner model, to determine the bulk modulus of monoclinic $Al_2Mo_3O_{12}$ (K_f) as 13.6± 2.6 GPa, which agrees with the ultrasonic results within the margin of error (*cf.* 3.2), validating the use of Turner's model.

Thermal stabilities of neat PE and VTMS-g-$Al_2Mo_3O_{12}$/PE composites have been evaluated from mass loss curves through parameters such as mass loss at 573 K, mass loss at 673 K, temperature corresponding to 10% mass loss (T_{10}) and temperature corresponding to 50% mass loss (T_{50}), as summarized in Table 1. Although the mass losses of neat PE at 573 and 673 K are low, 0.90 and 1.95 mass % respectively, the mass losses for all VTMS-g-$Al_2Mo_3O_{12}$/PE compositesare far lower. T_{10} and T_{50}parameters of VTMS-g-$Al_2Mo_3O_{12}$/PE composites are higher than for neat PE, however, the filler impact on these two parameters was not as significant as observed for the mass losses until 673 K. On the other hand, the effect of VTMS-g-$Al_2Mo_3O_{12}$ filler on melting temperature (T_m) of the composites, as evaluated by DSC curves, was negligible (Table 1). To evaluate the effect of VTMS-g-$Al_2Mo_3O_{12}$ filler on degree of crystallinity (X_c) of PE matrix, enthalpy change of melting (ΔH) was determined for all composites and their degrees of crystallinity were calculated considering $\Delta H^* = 273 Jg^{-1}$ for completely crystallized PE [54]using:

$$X_c = \frac{\Delta H}{\Delta H^* (1 - w_f)}. \quad (5)$$

where w_f is the mass fraction of filler.

This evaluation showed that VTMS-g-$Al_2Mo_3O_{12}$/PE composites lost some crystallinity, from ~76% for neat PE to ~70% for VTMS-g-$Al_2Mo_3O_{12}$/PE composite reinforced with 1 mass % of filler.

Young's moduli, yield strengths and yield strains of composites were determined from stress-strain curves and plotted in Figure 7. The stiffness and resistance to plastic deformation of the newcomposites both increased, as evidenced by an increase in Young's modulus, between 6.6 and 19.1 %, and yield strength, between 4 and 6 %. On the other hand, yield strain decreased between 8 and 12 % in comparison to neat PE.

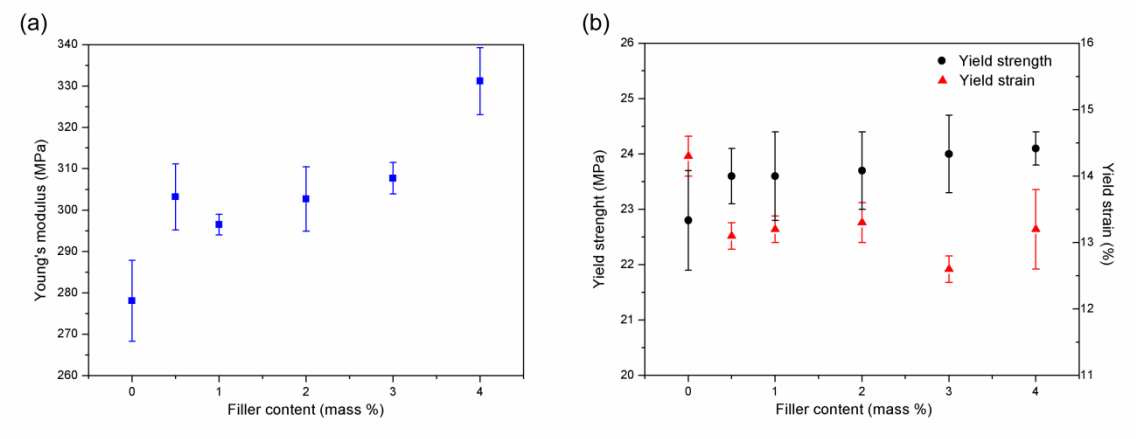

Fig.7 (a) Young's modulus; (b) Strength and strain at yield point of VTMS-g-$Al_2Mo_3O_{12}$/PE composites as a function ofnominal filler content

FEAwas used to calculate the thermal stresses experienced in the composites following a 100 K temperature drop, near room temperature. Cooling of the composites induces compressive thermal stresses in the VTMS-g-$Al_2Mo_3O_{12}$ and tensile thermal stresses in the PE matrix due to their mismatched CTEs. The compressive stress in the filler particles reached a maximum of 22 MPa, and was invariant with the filler loading. The maximum tensile and shear stresses in the PE matrix are shown in Figure 8. The maximum tensile stress increased approximately linearly with filler loading, while the maximum shear stress increasednonlinearly.

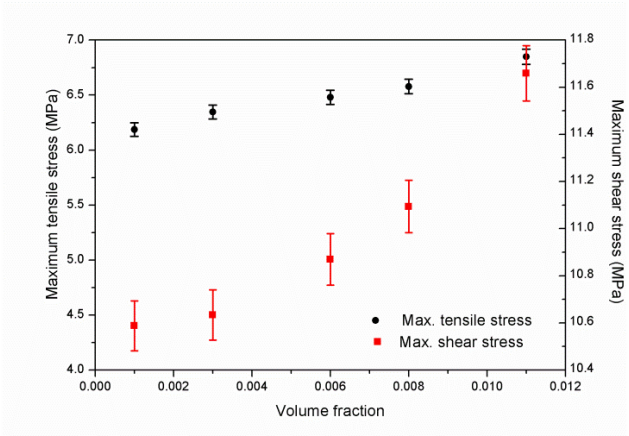

Fig.8 Maximum tensile and shear stresses in the PE matrix as a function of filler content. An estimated error due to finite mesh size of 1% is shown.

The CTE of the compositeon addition of filler was calculated to decrease only slightly, but more than would be predicted by the rule of mixtures. The discrepancy

between the finite element models and the experimental result is possibly due to the finite size of the model, which prevents accurate modelling of the constraint of the thermal expansion of the matrix due to the filler since the bulk of the matrix material is unconstrained.

4. Discussion

The mechanical properties of thermomiotics and low CTE materials still need to be more thoroughly studied, sincethis knowledge is fundamental for many potential applications. Thus far elastic constants and related properties such as bulk modulus (*K*) have been determined for several compounds from the $A_2M_3O_{12}$ family, in both orthorhombic and monoclinic structures[55-58]. Our analysis of experimental α_c versus volume filler fraction in terms of Turner's model (Figure 6) and calculationsbased on the ultrasonic testsgave a bulk modulus of 13.6 ± 2.6 GPa and 13.5 ± 1.3 GPa, respectively, for monoclinic $Al_2Mo_3O_{12}$, very close to the bulk moduli of monoclinic $Sc_2W_3O_{12}$, $Sc_2Mo_3O_{12}$, $In_2W_3O_{12}$ and $Zr_2WO_4(PO_4)_2$ of 11.8 ± 0.8 GPa, 16 ± 1 GPa, 13± 2 GPa and 17 ± 2 GPa, respectively, as determined from high pressure X-ray or neutron diffraction data.Only the bulk modulus of monoclinic $Al_2W_3O_{12}$ was reported to be higher (28 ± 1 GPa)[56], compared to other monoclinic phases. It is relevant for our study that Watanabe et al.,[18] estimated the bulk modulus of $Zr_2WO_4(PO_4)_2$ at 18 GPa, independently from theBirch-Murnaghan equation of state analysis of high-pressure X-ray diffraction data [57], and by applying Hashin's model on the relationship between experimental $Zr_2WO_4(PO_4)_2$/Mgcomposite bulk modulus and $Zr_2WO_4(PO_4)_2$ filler volume fraction, with excellent agreement for the two approaches. Monoclinic phases of the $A_2M_3O_{12}$ family are much softer than the corresponding orthorhombic phases, the ones that present NTE, withbulk moduli varying between 32 GPa for $Sc_2W_3O_{12}$ and$Sc_2Mo_3O_{12}$, and 48 GPa to 49 GPa for $Al_2W_3O_{12}$ and $Zr_2WO_4(PO_4)_2$, respectively[55-58]. In comparison, the bulk modulus of cubic α-ZrW_2O_8, the most studied thermomiotic filler, is much higher (~ 74 GPa)[59]. Although monoclinic $A_2M_3O_{12}$ phases have surprisingly low bulk moduli, even significantly lower than already soft NTE orthorhombic phases, note that, for example, $Al_2Mo_3O_{12}$ possesses a bulk modulus two orders of magnitude higher than polyethyleneused in this study, estimatedto be ~ 0.278 GPa. Therefore, in accordance to the Turner model, which

considers perfect interfaces between the two components [60], the high relative bulk modulus of $Al_2Mo_3O_{12}$ in comparison to the bulk modulus of PE would lead to a relevant reduction of composite CTE. Strong reduction of the CTE of the composite (as high as 46%) reached using filler contents not higher than 4 mass % (1.1 vol %) is a possible indication of efficient filler-matrix interaction through physical entanglements. It is worth noting that such a high reduction of composite CTE,obtained with low filler volume fractions, is reached in spite of the small decrease in crystallinity of the PE matrix with addition of VTMS-g-$Al_2Mo_3O_{12}$fillers (Table 1), indicating that the filler's thermal and mechanical properties, as well as the interfaces, dictate the overall composite properties.

These findings underline the importance of well-dispersed nanoparticles in the matrix as well as achievement of strong filler-matrix interactions, since the fulfillment of these conditions results in increased density of well-bonded interfaces in the composite per unit of volume, when compared to traditional non-functionalized micron size fillers. For instance, Dey and Tripathi [36] reported the influence of Si micron sized, chemically untreated, powder on thermal properties of Si/PE composites. Although the CTEof the Si/PE composite decreased with increased volume percentage of Si, the effect of filler content, as high as 20 vol %, on CTE of the composite was lower than that reached in VTMS-g-$Al_2Mo_3O_{12}$/PE composites with a volume filler content of 1.1 vol % (4 mass %). In agreement with the Si/PE result[36], Anjana et al., [38]achieved similar reduction of CTE to that reached here for 1.1 vol % VTMS-g-$Al_2Mo_3O_{12}$/PE composite by adding 30 vol % of non-functionalized micron size CeO_2 to the PE matrix. On the other hand, Sahebian et al.[34]reached a more pronounced decrease of CTE by adding to PE matrix a lower percentage (10 vol %) of nanometric $CaCO_3$ that had been pre-treated with stearic acid. They also observed that the variation of mean size of $CaCO_3$ nanoparticles mayplay a role in the CTE of $CaCO_3$/PE composites; i.e., nanopowders with smaller mean particle size act more efficiently to decrease the CTE of a composite than do nanopowders with higher mean particle size. However, it is relevant to notice that Sharma et al.[25] inferred that the CTE of ZrW_2O_8/polyimide composites was independent of the size of ZrW_2O_8 filler. They showed that the 5 vol % loading of nanometric or micronic ZrW_2O_8 fillers to polyimide (PI) matrix resulted in comparable CTE values. Sullivan and Lukehart[15] came to the same conclusion for the effect of 0.8 and 1.7 vol % loadings of nanometric and micronic ZrW_2O_8 fillers in a polyimide matrix. Sharma et al.[25]did not observe any additional

effect of ZrW_2O_8 nanofillers functionalized with 3-aminopropyltriethoxysilane or ZrW_2O_8 fillers functionalized with 3-aminopropyltriethoxysilane/PI oligomer on reduction of the composite CTE for loadings between 5 and 15 vol % when compared to non-functionalized ZrW_2O_8 nanofillers. Therefore, those authors suggested that a mechanism different from that usually ascribed for enhancement of mechanical and thermal properties of nanocomposites, such as good filler-matrix interaction, is responsible for governing thermal expansion in nanocomposites.

The thermal stability of VTMS-g-$Al_2Mo_3O_{12}$/PE composites was significantly increased at lower temperatures (< 673 K,Table 1), probably due to the joint action of (i) low permeability of fillers leading to a more tortuous path of diffused species, thereby decreasing the rate of gas evolution, and (ii) reduced movement of polymer chains due to the interactions between VTMS-g-$Al_2Mo_3O_{12}$ and the PE matrix [61]. Neat PE lost ~ 0.9 mass % on heating to 573 K, while the corresponding VTMS-g-$Al_2Mo_3O_{12}$/PE composites were essentially completely stable up to this temperature. Further temperature increases up to 673 K provoked a total mass loss of neat PE of ~ 2 mass %, while mass losses of VTMS-g-$Al_2Mo_3O_{12}$ composites were kept between 0.5 mass % (for 4 mass % VTMS-g-$Al_2Mo_3O_{12}$) and ~ 1 mass % (for1 mass % of VTMS-g-$Al_2Mo_3O_{12}$). In comparison, Chrissafis et al.[62]reported a mass loss of 1 mass % up to 548 K for $cSiO_2$ /PE composite with 2.5 mass % of filler ($cSiO_2$: functionalized SiO_2 nanofillers). Chrissafis and Bikiaris[61]reported that the addition of 2.5 mass % of montmorillonite nanoclays (MMT) or multiwalled carbon nanotubes (MWCNT) to PE matrix resulted in the same level of mass loss as their neat PE up to 573 K, ≤ 0.5 mass %.

The origin of thermal stability of nanocomposites with polymer matrices at high temperatures is not clear-cut since discrepant results have been reported, including decreases of thermal stability, especially for nanoclay fillers, due to the activation of different thermal degradation promoter mechanisms[61]. In the case of PE athigh temperatures (> 723 K), where the PE matrix degradation rate is high, a small increase of stability is confirmed, i.e., T_{10} and T_{50} were at most 6K and 3K higher, respectively, for VTMS-g-$Al_2Mo_3O_{12}$/PE composites with respect to neat PE. Here the increase of thermal stability at high temperatures (>723 K) is very similar to the value (~ 4K) observed by Chrissafis et al.[62]for a $cSiO_2$ /PE composite with 2.5 mass % of filler, judging from the temperature at which PE decomposition rate is highest. Similarly, a

rise of T_{10} of ~ 10 K was identified for the loadings < 5 mass % of non-functionalized micron-sized ZrW_2O_8 in PI matrix [21]. However, much higher increases in T_{10} and T_{50}, 25K and 21K, respectively, with respect to neat PE, were reported by Liao and Tjong[49]for 4 mass % VTMS-g-Al_2O_3/PE composite. Therefore, it seems that low or negative CTE fillers, like the majority of other inorganic fillers, do not promote thermal degradation of polyolefins or polyimide matrices, and are capable of increasing their thermal stability at high temperatures. In comparison, the thermal stability at high temperatures of silane-crosslinked PE could increase as much as 35 Kas reported by Aizan and Rahman[63]. Still, it is worth noting that in the future it would be relevant to understand the effect of nanofillers onevolution of VOCs from PE matrices modified by nanofillers, since the use ofPE for water pipe applications is negatively affected by the migration of VOCs to drinking water.

The degree of crystallinity of PE was little reduced with increasing content of VTMS-g-$Al_2Mo_3O_{12}$nanofillers (Table 1), from 76% (neat PE) to 70% (1mass % VTMS-g-$Al_2Mo_3O_{12}$/PE composite).Although it is commonly expected that nanofillers act only as heterogeneous nucleation sites, increasing the crystalline content of PE matrix, a steric hindrance effect of nanofillers on chain ordering, resulting in reduction of the crystallinity degree of PE has been reported[62, 64-66]. The hindrance effect of MWCNT[65], pristine and organofilized MMT [62], nano-SiO_2 and functionalized nano-SiO_2[62]and teak wood flour [66]on crystallization of PE is explained by the obstruction of fillers in PE chain ordering. Our results suggest that the same steric hindrance mechanism is responsible for the small reduction of the degree of crystallinity in thePE matrix when VTMS-g-$Al_2Mo_3O_{12}$ is added.The steric hindrance mechanism is actually a well-known tool in polymer processing, used to inhibit crystallinity of elastomers through addition of bulky methyl groups, rather than nanoparticles as here. Also, silane crosslinking of PE, using coupling agents such as VTMS, reduces the crystallinity of crosslinked PE due to steric hindrance[63]. Therefore, functionalized nanoparticles could serve as defect centers impeding chain ordering and, thus, reduce crystallinity of the PE matrix.

Melting temperature (T_m) was insensitive to the addition of nanofillers in polymeric matrices. Our findings showed negligible variation of melting temperatures of VTMS-g-$Al_2Mo_3O_{12}$/PE composites compared with $T_m$of neat PE (Table 1). Many other authors noticed asimilar lack of response of $T_m$in different composites with PE matrix and nanofillers. The list of fillers added to PE matrix that do not affect melting

temperature of composite is extensive. For example, Chrissafis et al. [62]reported this behavior for MWCNT, pristine and organofilized MMT, nano-SiO_2 and functionalized nano-SiO_2 , Li et al. [65]for MWCNT, Liao and Tjong [49]for Al_2O_3 and VTMS-g-Al_2O_3, Kanagaraj et al.[67]for MWCNT and Zebarjad et al. [68]for $CaCO_3$. The previously discussed decrease of crystallinity of the PE matrix in VTMS-g-$Al_2Mo_3O_{12}$/PE composites could reduce the sizes of crystal lamellae inPE spherulites. On the other hand, it is known that reduction of the average sizes of crystal lamellae decreases T_m of polymers. Therefore, it can be rationalized that negligible variation of T_m in VTMS-g-$Al_2Mo_3O_{12}$/PE composites is possibly due to the simultaneous action of two opposing effects: (i) size reduction of crystal lamellae inside spherulites causing a decrease of T_m and (ii) efficient filler-matrix interaction through physical entanglements contributing to an increase of T_m.

The mechanical properties of VTMS-g-$Al_2Mo_3O_{12}$/PE composites, such as Young's modulus and yield strength, were improved at room temperature in comparison to neat PE (Figure 7). The increase of Young's modulus (between 6.6 to 19.1 %), and yield strength (between 4 and 6 %) are a consequence of much higher elastic constants of monoclinic $Al_2Mo_3O_{12}$ in comparison to PE, but principally arises from the efficient load transfer from the PE matrix to the filler owing to the high density of strong filler-matrix interfaces, reached through physical entanglements. It is worth noting that the overall Young's modulus and yield strength of VTMS-g-$Al_2Mo_3O_{12}$/PE composites increased despite the reduction in the degree of crystallinity of PE matrixfor thecomposites, since it is well established that the increase of amorphous content in PE should lead to a decrease of mechanical properties of the matrix at the temperatures above the glass transition temperature (~ 163 K for PE). However, in VTMS-g-$Al_2Mo_3O_{12}$/PE composites the intimate interfacespermit load transfer, overriding the impact of decreasing crystallinity of PE matrix. On the other hand, there are opposite examples in the literature such as the report of Li et al. [65]which attributed the reduction of Young's modulus of MWCNT/PE composites to the decrease of crystallinity of PE matrix.

The reduction of yield strain,as observed for VTMS-g-$Al_2Mo_3O_{12}$/PE composites (Figure 7),has been reported for other composites with polymeric and metallic matrices. For example, Sharma et al. [25]reported a strong decrease of yield strain for 5 to 15 mass % additions inside PI matrix of ZrW_2O_8 nanofillers functionalized with 3-aminopropyltriethoxysilane or with 3-

aminopropyltriethoxysilane/PI oligomer. It should be noticed that even the addition of ductile Cu particles in a PE matrix [69]resultedin reduction of yield strain of Cu/PE composites.

The thermal stresses calculated by the finite element method for VTMS-g-$Al_2Mo_3O_{12}$/PE composites following cooling by 100 K(Fig. 8) were below the yield strength of the PE matrix (Fig. 7b) as well as the level that would be expected to affect the $Al_2Mo_3O_{12}$filler[9]. Therefore, the composites would be expected to be mechanically stable following thermal shock of 100 K or less, due to the absence of plastic deformation of the matrix or fracture of the $Al_2Mo_3O_{12}$ filler.However, addition of $Al_2Mo_3O_{12}$ in amounts considerably above 1.1 vol % might increase the thermal stress in the matrix above the yield strength of the PE due to the nonlinear increase in the thermal shear stress in the matrix. Although there is considerable CTE mismatch between PE and $Al_2Mo_3O_{12}$, the low stiffness of the matrix reduces the magnitude of the thermal stresses considerably, in addition to allowing reduction of the CTE by addition of only a small amount of filler.

5. Conclusions

This study investigated the viability of employinga nanometric $A_2M_3O_{12}$-typecompound, in low loadings (≤ 4 mass %), as a filler in a thermoplastic polymer in order to achieve considerable reduction of the matrix CTE, without causing adverse effects on themechanical properties and thermal stability. Nanometric $Al_2Mo_3O_{12}$, in the monoclinic form, grafted with VTMS, abi-functional coupling agent, was added to a PE matrix through melt-compounding extrusion and VTMS-g-$Al_2Mo_3O_{12}$/PE composites were fabricated by injection molding.

The as-prepared VTMS-g-$Al_2Mo_3O_{12}$/PE composites exhibited strong decrease of their CTEs, reaching 46 % reduction for loadings of 4 mass % (1.1 vol %). The results suggest efficient filler-matrix interaction through physical entanglements. Experimentally obtained CTEs of VTMS-g-$Al_2Mo_3O_{12}$/PE composites were successfully described by Turner's model and the bulk modulus of monoclinic $Al_2Mo_3O_{12}$ was calculated to be 13.6± 2.6 GPa, in good agreement with the bulk modulus of 13.5 ± 1.3GPa obtained by ultrasonic testing.

Thermal stability of VTMS-g-$Al_2Mo_3O_{12}$/PE composites was significantly increased at lower temperatures (< 673 K) in comparison to neat PE, while at high temperatures the increase was small, but not negligible. The degree of crystallinity of PE decreased a small extent with VTMS-g-$Al_2Mo_3O_{12}$ loading. However, the increased

amount of amorphous PE did not result in a significant change in melting temperature or deterioration of mechanical properties, the latter as judged by the Young's modulus and yield strength. Actually, the Young's modulus increased by 6.6 to 19.1 %, while the yield strength increased 4to 6 % owing to efficient load transfer from PE matrix to the fillers, because of the high density of strong filler-matrix interfaces.

This research shows the importance of further studies of low or negative CTE/thermoplastic composites.

Acknowledgments

B.A. Marinkovic and J.R.M. d'Almeida are grateful to CNPq (National Council for Scientific and Technological Development) for a Research Productivity Grants. Patricia I. Pontón is also grateful to CNPq for scholarship.M.A. White acknowledges support of NSERC through the Discovery Grants program. We thank J.W. Zwanziger for use of the ultrasonic transducer.

References

[1] Romao CP, Miller KJ, Whitman CA, White MA, Marinkovic BA(2013) Negative Thermal Expansion (Thermomiotic) Materials. In: Reedijk J, Poeppelmeier K(eds) Comprehensive Inorganic Chemistry II, vol. 4.Elsevier, Oxford, pp 127-151

[2] EvansJS, Mary TA, Vogt T, Subramanian MA, Sleight AW (1996) Negative thermal expansion in ZrW_2O_8 and HfW_2O_8,Chem Mater8:2809-2823.

[3] Evans J S, Mary TA, Sleight AW (1997)Negative thermal expansion in a large molybdate and tungstate family, J Solid State Chem133:580-583.

[4] Lind C, Wilkinson AP, Hu Z, Short S, Jorgensen JD(1998) Synthesis and properties of the negative thermal expansion material cubic $ZrMo_2O_8$,Chem Mater 10:2335-2337.

[5] EvansJS, Mary TA, Sleight AW (1998) Negative thermal expansion in $Sc_2(WO_4)_3$, J Solid State Chem 137:148-160.

[6] Evans JS, Mary TA (2000) Structural phase transitions and negative thermal expansion in $Sc_2(MoO_4)_3$, Int J Inorg Mater 2:143-151.

[7] Sumitra S, Waghmare UV, Umarji AM (2007) Anomalous dynamical charges, phonons, and the origin of negative thermal expansion in $Y_2W_3O_{12}$ Phys. Rev. B 76:024307.

[8] MarinkovicBA, Ari M, de Avillez RR, Rizzo F, FerreiraFF, Miller KJ, Johnson M B, White MA (2009) Correlation between AO_6polyhedral distortion and negative thermal expansion in orthorhombic $Y_2Mo_3O_{12}$ and related materials, ChemMater21:2886-2894.

[9] Prisco LP, Romao CP, Rizzo F, White MA, Marinkovic BA (2013) The effect of microstructure on thermal expansion coefficients in powder-processed $Al_2Mo_3O_{12}$, J Mater Sci 48:2986-2996.

[10] KimIJ andGauckler LJ (2008) Excellent thermal shock resistant materials with low thermal expansion coefficients,J Ceram Process Res 9:240-245.

[11] Shi JD, Pu ZJ, Wu KH, Larkins G (1997) Composite materials with adjustable thermal expansion for electronic applications,Mater Res Soc Symp Proc 445:229-234.

[12] Holzer H and Dunand DC (1999) Phase transformation and thermal expansion of Cu/ZrW_2O_8 metal matrix composites, J Mater Res14:780-789.

[13] Kofteros M, Rodriguez S, Tandon V, Murr LE (2001) A preliminary study of thermal expansion compensation in cement by ZrW_2O_8 additions, Scripta Mater 45:369-374.

[14] Tran KD, Groshens TJ, Nelson JG (2001) Fabrication of near-zero thermal expansion $(Fe_xSc_{1-X})_2Mo_3O_{12}$-$MoO_3$ ceramic composite using the reaction sintering process, Mater Sci and Eng A 303:234-240.

[15] Sullivan LM and Lukehart CM (2005) Zirconium tungstate (ZrW_2O_8)/Polyimide nanocomposites exhibiting reduced coefficient of thermal expansion, ChemMater17:2136-2141.

[16] Tani J, Kimura H, Hirota K, Kido H (2007) Thermal expansion and mechanical properties of phenolic resin/ZrW_2O_8composites, JAppl Polym Sci106:3343-3347.

[17] Goertzen WKand Kessler MR (2008) Three-phase cyanate ester composites with fumed silica and negative-CTE reinforcements, JTherm Anal Calorim 93:87-93.

[18] Watanabe H, Tani J, Kido H, Mizzuchi K (2008) Thermal expansion and mechanical propertis of pure magnesim containing zirconium tungsten phosphate particles with negative thermal expansion, Mater Sci Eng A 494:291-298.

[19] Yanase I, Miyagi M, Kobayashi H (2009) Fabrication of zero-thermal-expansion $ZrSiO_4/Y_2W_3O_{12}$ sintered body, J Eur Ceram Soc29:3129-134.

[20] Kanamori K, Kineri T, Fukuda R, Kawano T, Nishio K (2009) Low-temperature sintering of ZrW_2O_8-SiO_2 by spark plasma sintering, JMater Sci 44:855-869.

[21] Yang J, Yang Y, Qinqin L, Guifang X, Cheng X (2010) Preparation of negative thermal expansion ZrW_2O_8powders and its application in polyimide/ZrW_2O_8 composites, J Mater Sci Technol 26:665-668.

[22] Tani J, Takahashi M, Kido H (2010) Fabrication and thermal expansion properties of ZrW_2O_8/$Zr_2WP_2O_{12}$ composites, J Eur Ceram Soc 30:1483-1488.

[23] Lind C, Coleman MR, Kozy LC, Sharma GR (2011) Zirconium tungstate/polymer nanocomposites: challenges and opportuniteis, Phys Status Solidi B248:123-129.

[24] Chu X, Huang R, Yang H, Wu Z, Lu J, Zhou Y, Li L (2011) The cryogenic thermal expansion and mechanical properties of plasma modified ZrW_2O_8 reinforced epoxy,Mater Sci Eng A 528:3367-3374.

[25] Sharma GR, Lind C, Coleman MR (2012) Preparation and properties of polyimide nanocomposites with negative thermal expansion nanoparticle filler, MaterChemPhys137:448-457.

[26] YamashinaN, Isobe T, Ando S (2012) Low thermal expansion composites prepared from polyimide and ZrW_2O_8 particles with negative thermal expasion,JPhotopolym Sci Technol25:385-388.

[27] Wu Y, Wang M, Chen Z, Ma N,Wang H (2013) The effect of phase transformation on the thermal expansion property in Al/ZrW_2O_8 composites, JMater Sci48:2928-2933.

[28] Peng Z, Sun YZ, Peng LM (2014) Hydrothermal synthesis of ZrW_2O_8 nanorods and its application in ZrW_2O_8/Cu composites with controllable thermal expansion coefficients, MateDes54:989-994.

[29] Liu QQ, Cheng XN, Yang J, Sun XJ (2011) Influence of fabrication method on the structure and thermal expansion property of $ZrWMoO_8$ and its composites, JMater Sci 46:1253-1258.

[30] Suzhu Y, Hing P, Hu X (2000) Thermal expansion behaviour of polystyrene-aluminium nitride composites, J Phys D: Appl Phys 33:1606-1610.

[31] Wong CP and Bollampally RS (1999) Thermal conductivity, elastic modulus, and coefficient of thermal expansion of polymer composites filled with ceramic particles for electronic packaging,JApplPolym Sci 74:3396-3403.

[32] Take WA, Watson E, Brachman RW, Rowe RK (2012) Thermal expansion and contraction of geomembrane liners subjected to solar exposure and backfilling, JGeotech Geoenviron138:1287-1397.

[33] Skjevrak I, Due A, Gjerstad KO, Herikstad H (2003) Volatile organic components migrating from plastic pipes (HDPE, PEX and PVC) into drink water, Water Res37:1912-1920.

[34] Sahebian S, Zebarjad SM, Sajjadi SA (2010) Role of surface active agent on dimensional stability of HDPE/$CaCO_3$nanocomposites, J Thermoplast ComposMater 23:583-596.

[35] Baglari S, Kole M, Dey TK (2011) Effective thermal conductivity and coefficient of linear thermal expansion of high-density polyethylene - fly ash composites, Indian JPhys85:559-573.

[36]Dey T K and Tripathi M (2010) Thermal properties of silicon powder filled high-density polyethylene composites, Thermochim Acta502:35-42.

[37]Manu KM, Ananthakumar S, Sebastian MT (2013) Electrical and thermal properties of low permittivity $Sr_2Al_2SiO_7$ ceramic filled HDPE composites, CeramInt39:4945-4951.

[38]Anjana PS, Deepu V, Uma S, Mohanan P, Philip J, Sebastian MT (2010) Dielectric, thermal, and mechanical properties of CeO_2-Filled HDPE composites for microwave substrate applications, J Polym Sci, Part B: Polym Phys48:998-1008.

[39]Pöllänen M, Suihkonen R, Nevalainen K, Koistinen AP, Suvanto M, Vuorinen J, Pakkanen T (2012) Morphological, mechanical, tribological, and thermal expansion properties of organoclay reinforced polyethylene composites, Polym EngSci 53:1279-1286.

[40]Liu QQ, Cheng XN, Yang J (2012) Development of low thermal expansion $Sc_2(WO_4)_3$ containing composites, Mater Tech27:388-392.

[41]MarinkovicBA, Ari M, Jardim PM, de Avillez RR, Rizzo F, Ferreira FF (2010) $In_2Mo_3O_{12}$: A low negative thermal expansion compound, ThermochimActa499:48-53.

[42]Xiao XL, Cheng YZ, Peng J, Wu MM, Chen DF, Hu ZB, Kiyanagi R, Fieramosca JS, Short S, Jorgensen J (2008) Thermal expansion properties of $A_2(MO_4)_3$ (A = Ho and Tm; M = W and Mo), Solid State Sci 10:321-325.

[43]Ari M, Jardim PM, Marinkovic BA, Rizzo F, Ferreira FF (2008) Thermal expansion of $Cr_{2x}Fe_{22x}Mo_3O_{12}$, $Al_{2x}Fe_{22x}Mo_3O_{12}$ and $Al_{2x}Cr_{22x}Mo_3O_{12}$ solid solutions, JSolid State Chem181:1472-1479.

[44]Ari M, Miller KJ, Marinkovic BA, Jardim PM, de Avillez R, Rizzo F, White MA (2011) Rapid synthesis of the low thermal expansion phase of $Al_2Mo_3O_{12}$ via a sol–gel method using polyvinyl alcohol, JSol-Gel Sci Technol58:121-125.

[45]Pontón PI, d'Almeida JM, Marinkovic BA, Savic SM, Mancic L, Rey NA, Morgado EJr, Rizzo FC (2014) The effects of the chemical composition of titanate nanotubes and solvent type on 3-aminopropyltriethoxysilane grafting efficiency, Appl Surf Sci 301:315-322.

[46]Asmani M, Kermel C, Leriche A, Ourak M (2001) Influence of porosity on Young's modulus and Poisson ration in alumina ceramics, J Eur Ceram Soc21:1081-1086.

[47] http://www.paralab.pt/sites/default/files/pdf/DIL402C.pdf. Accessed 17 Feb 2014

[48]Kuznetsova A, Wovchko EA, Yates JT (1997) FTIR study of the adsorption and thermal behavior of vinyltriethoxysilane chemisorbed on γ-Al_2O_3, Langmuir13:5322-5328.

[49]Liao CZ and Tjong SC (2013) Mechanical and thermal perfomance of high-density polyethylene/alunima nanocomposites, J Macromol Sci, Part B: Phys52:812-825.

[50]Nguyen VG, Thai H, Mai HD, Tran HT, Tran DL, Vu M T (2013) Effect of titanium dioxide on the properties of polyethylene/TiO_2 nanocomposites, Composites Part B45:1192-1198.

[51]Abboud M, Turner M, Duguet E, Fontanille M (1997) PMMA-based composite materials with reactive ceramic fillers Part 1.—Chemical modification and characterisation of ceramic particles, J Mater Chem7:1527-1532.

[52]Byrne MT, McCarthy EJ, Bent M, Blake R (2007) Chemical functionalisation of titania nanotubes and their utilisation for the fabrication of reinforced polystyrene composites, JMater Chem 17:2351-2358.

[53]Guo Z, Pereira T, Choi O, Wang Y, Hahn HT (2006) Surface functionalized alumina nanoparticle filled polymeric nanocomposites with enhanced mechanical properties, J Mater Chem16:2800-2808.

[54]Gao J-g, Yu M-s, Li Z-t (2004) Nonisothermal crystallization kinetics and melting behavior of bimodal medium density polyethylene/low density polyethylene blends, Eur Polym J44:1533–1539.

[55]Varga T, Wilkinsin AP, Jorgensen JD, Short S (2006) Neutron powder diffraction study of the orthorhombic to monoclinic transition in $Sc_2W_3O_{12}$ on compression, Solid State Sci 8:289-295.

[56]Varga T, Wilkinson AP, Lind C, Bassett WA, Zha C (2005) High pressure synchrotron x-ray powder diffraction study of $Sc_2Mo_3O_{12}$ and $Al_2W_3O_{12}$, JPhys:CondensMatter17:4271-4283.

[57]Baiz TI, Heinrich PC, Banek NA, Vivekens BL, Lind C (2012) In-situ non-ambient X-ray diffraction studies of indium tungstate, JSolid State Chem 187:195-199.

[58]Cetinkol M, Wilkinsion AP, Lind C (2009) In situ high-pressure synchrotron x-ray diffraction study of $Zr_2(WO_4)(PO_4)_2$ up to 16 GPa, PhysRev B79:224118.

[59]Drymiotis FR, Ledbetter H, Betts JB, Kimura T, Lashley JC, Migliori A (2004) Monocrystal elastic constants of the negative-thermal-expansion compound zirconium tungstate (ZrW_2O_8), Phys Rev Lett93:025502.

[60]Takenaka K (2012) Negative thermal expansion materials: technological key for control of thermal expansion, Sci Technol Adv Mater 13:013001.

[61]Chrissafis K and BikiarisD (2011) Can nanoparticles really enhance thermal stability of polymers? Part I: An overview on thermal decomposition of addition polymers,Thermochim Acta, 523:1-24.

[62]Chrissafis K, Paraskevopoulos KM, Tsiaoussis I, Bikiaris D (2009) Comparative study of the effect of different nanoparticles on the mechanical properties, permeability, and thermal degradation mechanism of HDPE, JAppl PolymSci 114:1606-1618.

[63]Aizan W and Rahman WA (2006) Design of silane crosslinkable high density polyethylene compounds for automotive fuel tank application. Proyect Report, Universiti Teknologi Malaysia.

[64]Tjong SC (2006) Structural and mechanical properties of polymer nanocomposites, Mater Sci Eng R53:73-197.

[65]Li S, Chen H, Cui D, Li J, Zhang Z, Wang Y, Tang T (2010) Structure and properties of multi-walled carbon nanotubes/polyethylene nanocomposites synthesized by in situ polymerization with supported Cp_2ZrCl_2 catalyst, Polym Compos 31:507-515.

[66]Sewda K and Maiti SN (2009) Mechanical properties of teak wood flour-reinforced HDPE composites, J ApplPolym Sci112:1826-1834.

[67]Kanagaraj S, Varanda FR, Zhil'tsova TV, Oliveira MS, Simões JAO (2007) Mechanical properties of high density polyethylene/carbon nanotube composites, Compos SciTechnol 67:3071-3077.

[68]Zebarjad SM, Sajjadi SA, Tahani M, Lazzeri A (2006) A study on thermal behaviourof HDPE/$CaCO_3$ nanocomposites, J Achiev Mater Manuf Eng 17:173-176.

[69]Tavman IH (1997) Thermal and mechanical properties of copper powder filled poly(ethylene) composites, Powder Technol 91:63-67.